INTERACTION OF AN IDEALIZED CYCLONE WITH A WAVY MIDLATITUDE JET

by

Brian Foster

A Thesis Submitted in

Partial Fulfillment of the

Requirements for the Degree of

Master of Science

in Atmospheric Science

at

The University of Wisconsin-Milwaukee

May 2025

ABSTRACT

INTERACTION OF AN IDEALIZED CYCLONE WITH A WAVY MIDLATITUDE JET

by

Brian Foster

The University of Wisconsin-Milwaukee, 2025
Under the Supervision of Professor Sergey Kravtsov

Numerical weather prediction model forecasts of the Rossby wave packets (RWP) initiated from the interaction of a tropical cyclone and a midlatitude jet stream are often characterized by decreased accuracy and lowered forecast skill. Factors influencing the level of interaction between a tropical cyclone (TC) and a midlatitude jet depend on the size, strength, and location of the TC relative to the jet, along with the meridional extent, wave pattern, and speed of the jet, especially when interacting with an upstream trough. This study uses a bare-bones (quasi-geostrophic) model to simulate and analyze the evolution of RWPs originating from the interaction of an idealized, constant-shape TC with a prescribed stationary wave pattern in a mid-latitude jet. The goal of this study is to map out the sensitivity of the TC's downstream impacts on the jet to the TC's initial position, the width and the degree of initial waviness of the jet, as well as the relative strength of the jet and the TC. Our model setup is based on earlier idealized studies of interactions of the midlatitude jet with topography which offer an explanation of the nonlinear dynamics behind zonal and blocked mid-latitude flow regimes. The TC is to be included in the overall system as a singular vortex (SV), which provides unambiguous separation of the vortex field from the ambient field and the separation between the background flow and RWPs generated by the SV, with RWPs created from this interaction leading both to the SV's self-propagation and to the downstream perturbations of the jet.

TABLE OF CONTENTS

LIST OF FIGURES

LIST OF TABLES

1. Introduction

1a) Literature Review

Tropical cyclones (TCs) undergoing extra-tropical transition (ET) (Jones et al. 2003, Evans et al. 2017, Keller et al. 2019) have been proven to create drastic changes in the midlatitude flow far downstream of their initial interaction with the mid-latitude jet through the Rossby-wave packets (RWP) these interactions generate (Fig. 1) (Wirth et al. 2018, among others). In the Atlantic sector, for example, the latter wave packets form or enhance deep ridges and troughs that may lead to high-impact weather events over Europe (e.g., Grams and Blumer 2015). In an analogous way, severe downstream weather can result from TC interaction with the mid-latitude jet in the Pacific sector. A well-known illustration of this process is the case of super typhoon Nuri, whose interaction with the midlatitude jet in eastern Asia produced a ridge-trough couplet over North America, which forced western North America into a heat wave while simultaneously pummeling eastern North America in a cold snap with snowfall in some areas (Keller et al. 2019).

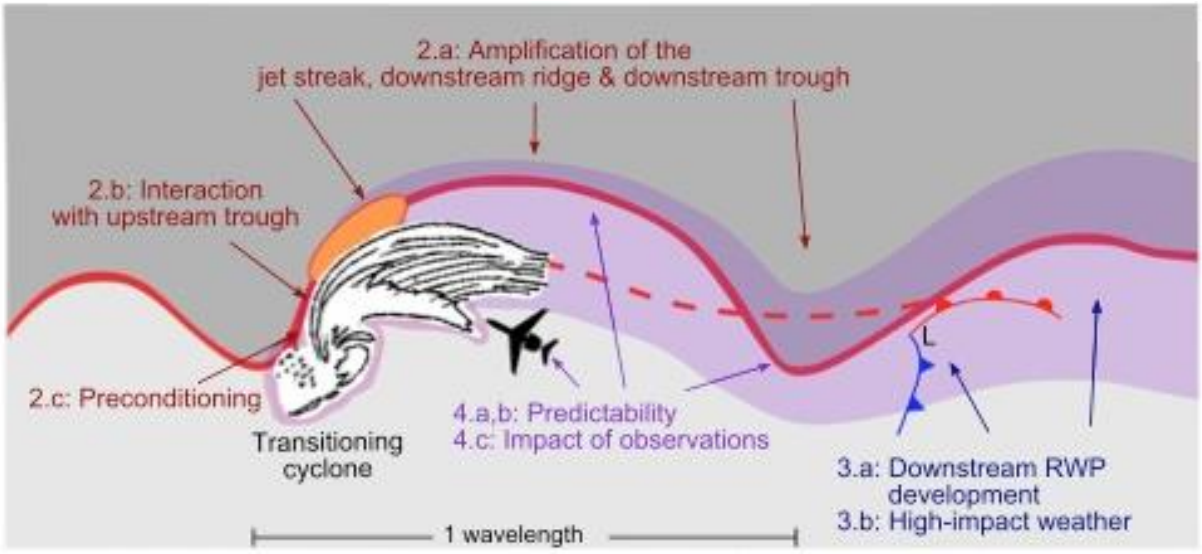

Figure 1: An overview of synoptic-scale features and processes associated with Northern Hemisphere ET events, focusing on downstream development triggered by the interaction of a TC (labeled "Transitioning

Cyclone") with an upstream trough and midlatitude jet streak (located along the thick red line). Reproduced from Fig. 2 of Keller et al. (2019).

The development of such RWPs has been previously considered in a range of numerical models of different complexity (Ferreira and Schubert 1999; Schwierz et al. 2004; Riemer et al. 2008). In the most realistic models, the magnitude of the RWP downstream amplification appears to depend primarily on three factors (Keller et al. 2019). The first is the amount of moisture transported poleward by the tropical cyclone. Greater moisture content is associated with stronger latent heating in deep, moist convection that, in turn, decreases upper-tropospheric PV, in turn strengthening the ridge downstream of the transitioning cyclone and creating greater RWP amplification. The second is the strength of the upper-tropospheric midlatitude jet stream (e.g., Finocchio and Doyle 2019). A weaker jet is more susceptible to meridional amplification by ET, and consequently, more likely to undergo Rossby wave breaking, increasing the local impact of the transitioning cyclone but reducing its impact downstream. The third and most suggested important factor that governs the RWP amplification is the phasing between the transitioning tropical cyclone and the upstream trough (e.g., Archambault et al. 2013, 2015; Wirth et al. 2018; Keller et al. 2019). The phasing is simply the extent to which the tropical cyclone during ET is positioned, relative to the midlatitude jet stream, in a favorable environment for non-tropical cyclone development. Stronger phasing, especially in the case of phase-locking when midlatitude potential vorticity advection promotes prolonged in-phase motion with the upstream trough, results in a stronger, more pronounced interaction between the cyclone and the environment (Keller et al. 2019), enhancing RWP amplification.

Global numerical weather models today exhibit decreased accuracy in forecasting the downstream impacts of the interaction between a developing extra-tropical cyclone (ETC) and the midlatitude flow several days in advance (Jones et al. 2003), with the sensitivity stemming

from all of the three factors outlined above. For example, Aiyyer (2015) and Keller et al. (2019) found that RWPs forecasted in the presence of interaction of the developing ETC with a pre-existing upstream trough are often underestimated in strength, which also translates into large forecast errors in weather conditions downstream (Aiyyer 2015, Evans et al. 2017).

1b) Study Purpose and Goals

While the long-term goal of the present project is to contribute to our understanding of the limitations and, possibly, to improve the skill of modern numerical weather prediction models in predicting high-impact weather downstream of a TC interacting with the mid-latitude jet, our immediate goal is to explore basic dynamics of the vortex embedded in a wavy jet-stream within a minimal setting. In particular, following previous idealized studies of the interactions of the midlatitude jet with either topography (Charney and DeVore 1979) or an isolated vortex (Reznik 1992), we neglect the diabatic and baroclinic processes and explore the barotropic mechanisms of downstream amplification of RWP generated by an idealized TC depending on the strength, width, and the degree of waviness of the pre-existing wave-2 jet, as well as the strength, size and initial location of the TC with respect to this jet. This arrangement mimics, in an idealized fashion, a climatological set up of the atmospheric mid-latitude circulation in the Northern Hemisphere (cf. Fig. 1), where the wave-2 structure arises due to a combination of the actual and "thermal" (land–sea contrast) topography, viz. the two major mountain ranges and the two land masses separated by two oceans. In section 2 below, we formulate the proposed model, and describe essential earlier results. The results of our analysis are presented in section 3, where we first describe the model tuning and sensitivity tests in the absence of the TC vortex (section 3a). These analyses are used to map out a suite of plausible wavy basic states to provide the background flow in which the TC evolution will occur (section 3a). Section 3b analyzes the TC

trajectories and the perturbations of the background flow that are caused by the interaction of the vortex with this flow, focusing on the sensitivity of this behavior to the model's multiple control parameters, including the strength of the vortex, width and intensity of the jet, and the initial placement of the vortex with respect to the climatological stationary wave. Section 4 will sum up the results and outline potential future studies.

2. Model Formulation and Background Information

Our proposed model is a classical 1.5-layer model describing the conservation of the quasi-geostrophic potential vorticity on an (x, y) infinite-extent β-plane:

$$\left(\nabla^2\hat{\psi} - a^2\hat{\psi}\right)_t + \beta\hat{\psi}_x + J\left(\hat{\psi}, \nabla^2\hat{\psi} - a^2\hat{\psi} + f_0 h_0 \hat{h}\right) = -D\nabla^2\left(\hat{\psi} - \bar{\psi}\right) + a^2 r\left(\hat{\psi} - \bar{\psi}\right). \quad (1)$$

Here $\hat{\psi}(x, y, t)$ is the quasi-geostrophic streamfunction (t is time), a is the inverse Rossby radius of deformation R_d, the beta-parameter β is the derivative of the Coriolis parameter with respect to y, f_0 is the reference value of the Coriolis parameter, $\hat{h}(x, y)$ is the dimensionless bottom topography, with the scale of $h_0 = h^*/H$<1 (h^* is the dimensional mountain height, H is the atmospheric scale height), r and D are the inverse time scales of the zonal-flow relaxation to the radiative equilibrium flow profile $\bar{\psi}(y)$ (which is assumed to be a function of latitude only, following Charney and DeVore 1979), with the former modeling radiative relaxation and the latter — frictional drag at the surface, subscript *t* denotes the time derivative, while ∇^2 and J are the Laplacian and *J*acobian operators, respectively.

We further decompose the streamfunction $\hat{\psi}$ as follows:

$$\hat{\psi} = \bar{\psi}(y) + \tilde{\psi}(x, y, t), \quad (2)$$

and assume that the perturbation $\tilde{\psi}(x, y, t) \to \langle\tilde{\psi}\rangle$ at infinity (so that the deviations of $\tilde{\psi}$ from the zonal mean there vanish). We also assume that $h(x, y)$ vanishes at infinity as well. In the

absence of the bottom topography $h_0 = 0$, $\hat{\psi} = \bar{\psi}(y)$ is the exact solution of (1), and, thus, in this steady state, $\tilde{\psi} = 0$. Substituting (2) in (1) gives

$$\left(\nabla^2\tilde{\psi} - a^2\tilde{\psi}\right)_t + \beta\tilde{\psi}_x + J\left(\bar{\psi} + \tilde{\psi}, \nabla^2\left(\bar{\psi} + \tilde{\psi}\right) - a^2\left(\bar{\psi} + \tilde{\psi}\right) + f_0 h_0 \hat{h}\right) \quad (3)$$

$$= -D\nabla^2\tilde{\psi} + a^2 r\tilde{\psi}.$$

The above equation (3), with the initial condition $\tilde{\psi}(x, y, 0) = 0$, describes the adjustment of the initially zonally uniform flow to the presence of the localized topographic zonal asymmetries with $h_0 > 0$. We expected that (3) is characterized by rich non-linear dynamics leading to the multiple equilibria (viz. zonal and blocked regimes: see **Fig. 2**) and time-dependent solutions for the parameter choices in which a strong climatological jet coexists with a pronounced topography (cf. Charney and DeVore 1979; Legras and Ghil 1985), but these expectations didn't pan out (see section 3a).

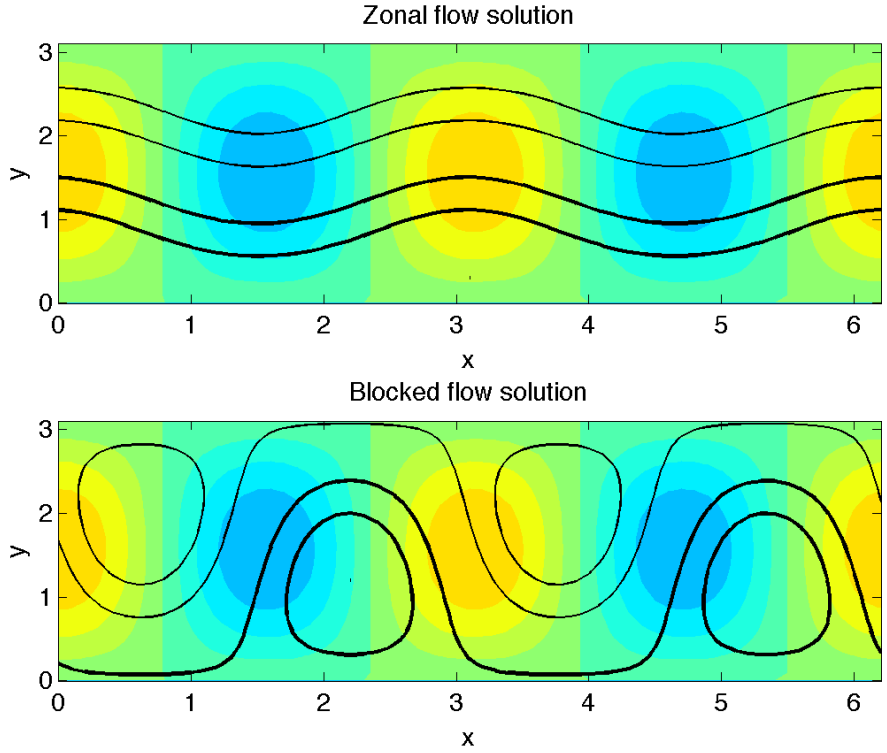

Figure 2: Zonal (top) and blocked (bottom) flow streamfunction (positive contours heavy, negative – light) in a three-mode truncation of (3) with wave-2 sinusoidal topography (shading: yellow/blue colors correspond to mountains/dips with respect to the mean level). Adapted from Charney and DeVore (1979).

The main goal of the proposed work is to understand interactions of a vortex with a wavy mid-latitude flow generated by model (3). To do so, we will adopt the singular vortex (SV) approach (Reznik 1992; Kravtsov and Reznik 2019, 2021; Reznik and Kravtsov 2021). This approach is motivated by an observation that salient aspects of the multi-scale atmospheric interactions involving eddies may be insensitive to the detailed spatial structure of the individual eddies (Löptien and Ruprecht 2005; Kravtsov and Gulev 2013; Kravtsov et al. 2015). This observation suggests that multi-scale midlatitude atmospheric variability may be understood by considering the systems of interacting vortices whose profiles contain a singularity at the center of the vortex; in such systems, the singular eddy field is clearly isolated from the regular field, thereby allowing unambiguous identification of the various dynamical components of the eddy–mean-flow interaction. A key assumption in this formulation is that the singular vortex does not dissipate; it is equivalent to assuming that the constant-shape singular vortex is maintained by dynamical balances unresolved by the model (e.g., moist thermodynamic processes); this assumption is supported by the tendency of the vortices to retain their coherence despite the deformation effect of the ambient flow (Schwierz et al. 2004).

Specifically, we introduce, on top of a large-scale flow, an additional localized perturbation in the form of the singular Bessel vortex (hereafter, SV) and thus decompose the full disturbance $\tilde{\psi}$ into the sum of a regular and singular components ψ and ψ_s (following Reznik 1992; Reznik and Kizner 2010):

$$\tilde{\psi} = \psi + \psi_s,\ \psi_s = -\frac{A}{2\pi} K_0(p|\boldsymbol{r} - \boldsymbol{r}_0(t)|). \tag{4}$$

Here K_0 is the modified Bessel function of the zeroth order, the pre-specified parameters A and $p > 0$ are constant, A governs the sign and integral intensity of the SV, p is the inverse of the horizontal scale of the vortex $L_v = p^{-1}$. The SV moves along the trajectory $\boldsymbol{r} = \boldsymbol{r}_0(t)$, starting from an arbitrary initial position $\boldsymbol{r}_0(0)$. Under heuristic assumptions that the zonal damping term on the right-hand side of (3) only acts on a large-scale flow, and that the SV is able to maintain its constant shape via dynamics unresolved in the present model, the substitution of (4) into (3) results in the following system of equations:

$$(\nabla^2\psi - a^2\psi)_t + \beta(\psi + \psi_s)_x + J\big(\bar{\psi} + \tilde{\psi}, \nabla^2\psi + \bar{\psi}_{yy} - a^2(\psi + \bar{\psi}) + f_0 h_0 \hat{h}\big) \qquad (5a)$$

$$-J\big(\nabla^2\psi + \bar{\psi}_{yy} - p^2(\psi + \bar{\psi}) + f_0 h_0 \hat{h}, \psi_s\big) + (p^2 - a^2)J(\dot{x}_0 y - \dot{y}_0 x, \psi_s) =$$

$$(-D\nabla^2 + a^2 r)\psi,$$

$$\dot{x}_0 = -(\psi + \bar{\psi})_y\big|_{\boldsymbol{r}=\boldsymbol{r}_0(t)}, \qquad \dot{y}_0 = (\psi + \bar{\psi})_x\big|_{\boldsymbol{r}=\boldsymbol{r}_0(t)}, \qquad \psi|_{t=0} = \psi_I,\ \boldsymbol{r}_0(0) = \boldsymbol{r}_I. \qquad (5b,c,d)$$

Here (5a) describes the evolution of the field ψ, hereafter called the induced (by either topography or the SV) streamfunction, and (5b–d) describe the motion of the SV. The system (5) was studied in the absence of topography ($h_0 = 0$) and in the limit of vanishing large-scale damping ($D = r = 0$) by Kravtsov and Reznik (2023) and Reznik and Kravtsov (2024) in the context of the zonally uniform background flows (see an example below). Naturally, the equation (5a) in the system without the SV ($A = 0 \rightarrow \psi_s = 0$) reduces to (3), since all the additional terms involving ψ_s vanish. Equations (5b–d) in this case describe an arbitrary trajectory of a passive tracer.

The system (5) is solved numerically — using a finite-difference formulation developed and used in Kravtsov and Reznik (2019, 2021), Reznik and Kravtsov (2020, 2021) — in a domain formally approximating an infinite plane but, technically, set up as a channel model with

large zonal and meridional extent, in which the zonal-jet forcing, mountain ranges and a vortex are all located far away from the channel boundaries and mimic the geometry and feature scales of the atmospheric circulation in the Northern Hemisphere.

Table 1: Fixed dimensional parameters used in the numerical experiments.

Parameter	Parameter description
$R_d = 600$ km	Rossby radius of deformation
$f_0 = 10^{-4}$ sec^{-1}	Coriolis parameter
$\beta = 2 \times 10^{-11}$ m^{-1} sec^{-1}	y-gradient of the Coriolis parameter
$\Delta x = \Delta y = \Delta = R_d/24 = 25$ km	Model resolution (spatial grid size)
$L_x = 1024\Delta$=25600 km	x-extent of the channel
$L_y = 1200\Delta$=30000 km	y-extent of the channel
T =80 days	Duration of most of the simulations
$\Delta t = 20$ sec	Time step
$A = 2\pi\beta R_d^3 \times (5, 10, 15)$	SV intensity
L_v: 300 km	SV size: small-vortex case
L_v: 600 km	SV size: intermediate-size-vortex case
L_v: 1200 km	SV size: large-vortex case
$m = 0.3, 0.5, 1$	wide jet, intermediate-width, narrow jet
$U_0 = 15, 20, 25$ m/s	Background-flow strength
$m_1, m_2 = 0.3, 0.5,\ h_0 = 0.3, 0.5, 0.7$	Orography parameters (width and height)
$D = 1/5$ day^{-1}	Surface drag parameter
$r = 1/10$ day^{-1}	Radiative relaxation parameter

In particular, for both the zonal background flow and topography profiles we will use the hyperbolic functions as follows:

$$\bar{\psi}(y) = -\frac{U_0}{m}\tanh my, \quad U(y) = -\bar{\psi}_y = \frac{U_0}{\cosh^2 my}, \tag{6a}$$

$$\hat{h}(x,y) = \hat{h}^{(x)}\hat{h}^{(y)}, \tag{6b}$$

$$\hat{h}^{(y)} = \frac{1}{\cosh^2 m_1 y}, \qquad \hat{h}^{(x)} = \frac{1}{\cosh^2 m_2(x-x_1)} + \frac{1}{\cosh^2 m_2(x-x_2)},$$

where the (x, y) coordinates have the origin in the center of the channel and are normalized by the Rossby radius R_d. The suggested values of parameters used here, along with other model parameters are listed in Table 1. The resulting configuration illustrated in **Fig. 3** features a channel about twice as long as the extent of the latitudinal circle at 45°N and about three times as wide as the meridional extent from the equator to the North Pole, but the jet and orography parameters quantitatively match the actual typical sizes and the relative feature arrangement within the Northern Hemisphere. An important alternative modification of this geometry would be to limit the zonal extent of the channel and explore the role of the global modes of variability — whose existence centrally involves the periodic boundary conditions in the zonal direction — in the dynamics of the problem considered (see, for example, Swanson 2008).

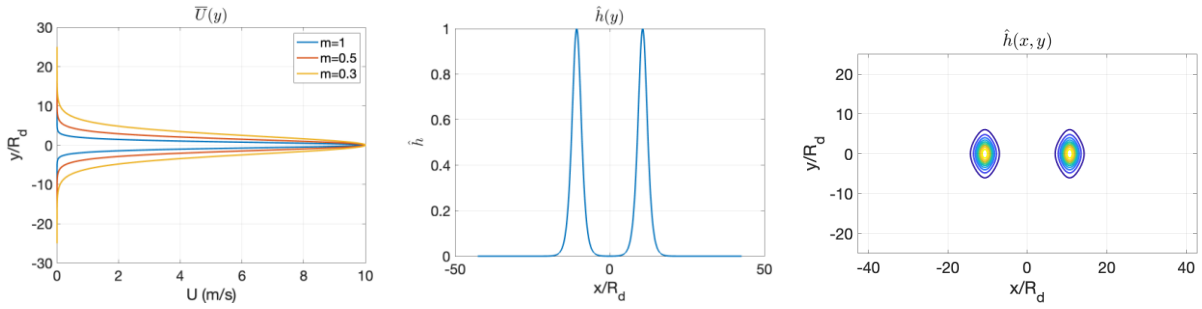

Figure 3: The proposed background-flow and orography profiles. Left: background-flow (6a) zonal velocity (m/s); right: the meridional cross-section and two-dimensional pattern of the model orography (6b).

An example of the simulation, using the model above, of a single TC-like vortex interacting with a straight jet (the case with no topography: Kravtsov and Reznik 2024) is shown in **Fig. 4**. The hyperbolic jet (6a), with $m = 0.5$, chosen to provide a stable large-scale configuration in the absence of the cyclone, flows along the axis of the channel, with a maximum wind U_0 of 10 m/s,

the width (the distance between the latitudes at which the wind is equal to $U_0/2$) is about 3000 km, the 'radius' of the singular cyclone is equal to Rossby scale R_d of 600 km (in this case the PV associated with the cyclone is a delta-function). Initially, at time minus 6 hours, the cyclone is placed at the latitude of $U_0/2$ on the jet's southern flank (not shown). The SV then generates a RWP, resulting in the SV's crossing the jet. The simulated evolutions of both the SV cyclone and

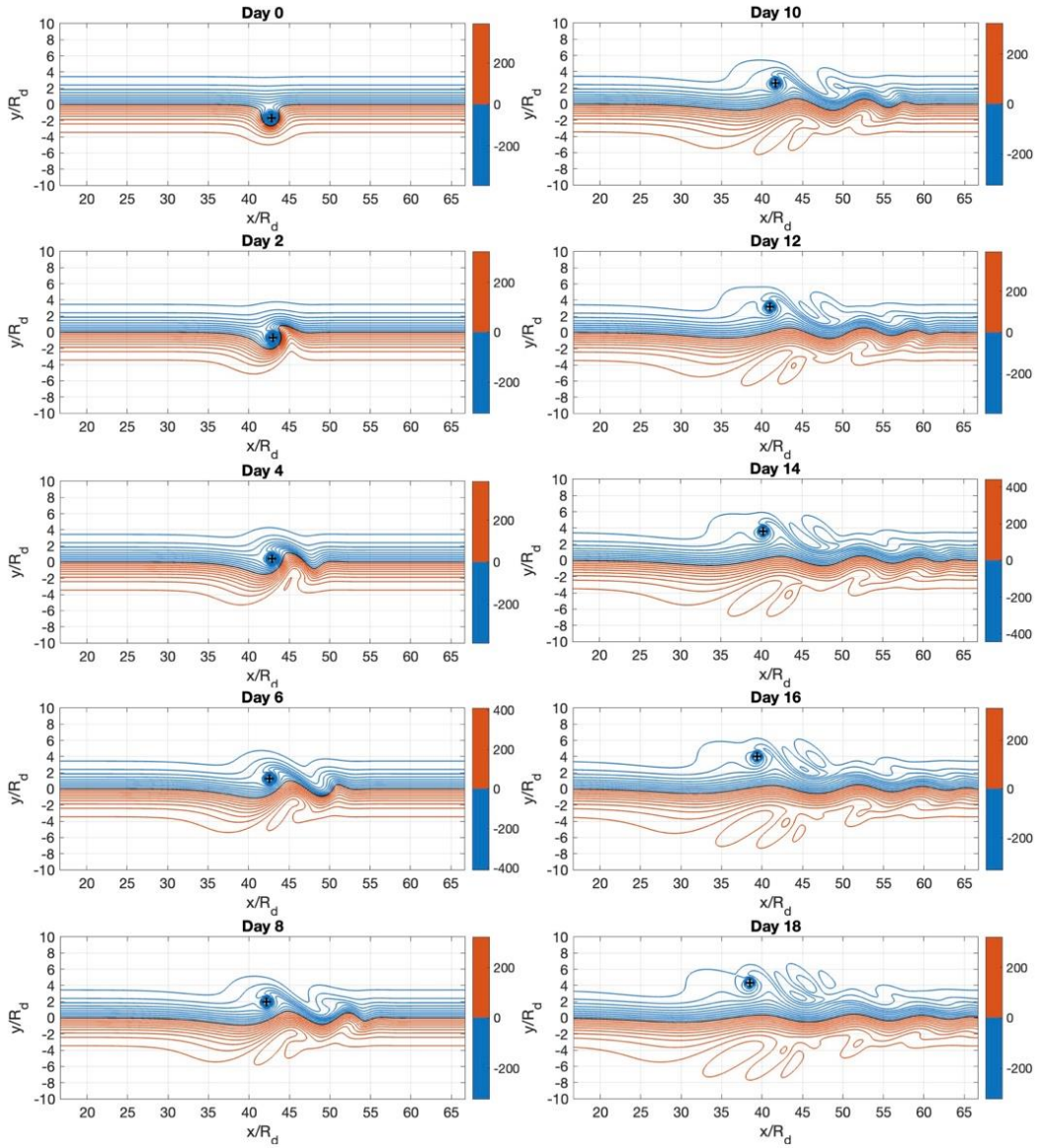

Figure 4: Jet crossing by a singular TC-like vortex in a highly idealized, 1.5-layer beta-plane quasi-geostrophic model of atmospheric circulation set up in a zonal channel. The cyclone is initially placed on the southern flank of the jet and is self-propelled across the jet by a secondary regular field of Rossby waves radiated by the cyclone. Shown is the full streamfunction field at different times listed in the caption of each panel. The streamfunction units are $U\Delta x$, where the velocity scale $U = 10\text{ms}^{-1}$ and

Δx=25km is the spatial grid size. The zonal and meridional coordinates *x* and *y* are nondimensionalized using the Rossby scale taken here to be $R_d = 600$km.

its induced downstream development are somewhat reminiscent of the weak-jet scenario considered by Riemer et al. (2008), although their "weak" straight jet was much more intense (27 m/s rather than 10 m/s) and they used a full-physics model. In the present formulation, however, separating the cyclone itself, mean flow, and the regular Rossby-wave field induced by the cyclone is trivial since the mean flow is fixed and the cyclone's streamfunction is easily reconstructed using its fixed singular profile and a known position of the cyclone at each time, which is predicted by the model.

3. Results

The goal of this project is to map out different possible regimes of interaction between a wavy mid-latitude jet and a TC in the context of the basic barotropic formulation (4–6). A particular hypothesis we aim to address is that the downstream impacts of TC will be dependent on the initial zonal position of the vortex with respect to the climatological stationary wave. To model a dynamically consistent climatological stationary wave, we'll first generate a set of steady-state solutions without the vortex (*A*=0) for various strengths and widths of the background-state jets and topography of different heights (see Table 1). These states are discussed below in section 3a. Then, in section 3b, we'll provide a detailed account of interactions between the idealized TCs of different intensities and these background states. These results are summarized and further discussed in section 4.

3a. Stationary Waves

The most pronounced stationary waves were obtained for the parameter set associated with the highest topography $h_0 = 0.7$ and largest jet speed $U_0 = 25$ m/s. The corresponding steady-state solutions for the cases of narrow, standard, and wide jets are shown in **Figs. 5a–c**, respectively. These solutions, visually, are a combination of the wave-2 and wave-4 patterns, with main troughs located immediately downstream of each mountain and the secondary troughs — farther downstream, roughly halfway between the mountains. The zonal undulations of the jet increase in geometrical size and magnitude with the jet's width. In particular, the narrow-jet solution (Fig. 5a) is characterized by the weakest wave, with the most localized troughs which only exhibit a slight eastward shift with respect to the mountain peak, and a very shallow secondary troughs that are somewhat closer to the upstream mountain. At the same time, the wide jet's solution (Fig. 5c) has the strongest wave, with the largest-scale troughs, which are all located a bit further downstream (eastward) compared to their narrow-jet counterparts. This includes both the main troughs on the lee side of the mountains and the secondary troughs between the mountains; the latter troughs are now located closer to the downwind mountain.

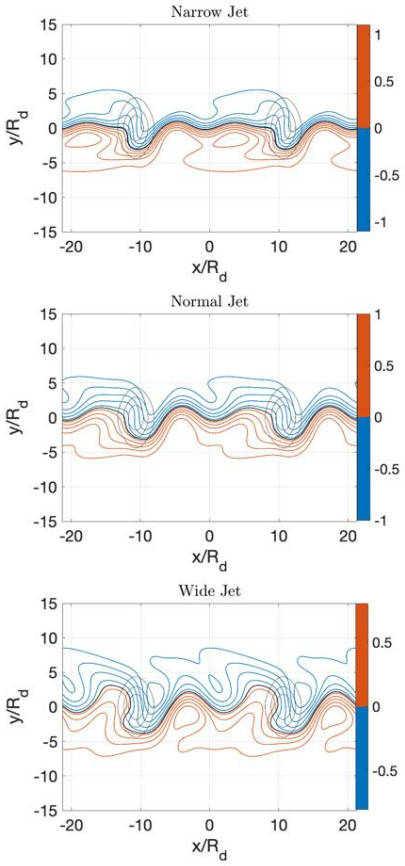

Figure 5: The steady-state solutions of the system (4–6) without the vortex (A=0) for the case with $h_0 = 0.7$ and $U_0 = 25$ m/s. Shown is dimensionless streamfunction in units of $U_0 R_d / m$. The zonal and meridional coordinates x and y are nondimensionalized using the Rossby scale taken here to be $R_d = 600$km. Mountains are shown as black contours with the contour interval of 0.2.

The stationary waves above are different from those obtained in similar models by Charney and Eliassen (1949) and Charney and DeVore (1979). This is possibly because these authors used an effectively coarser-resolution spectral truncation of the model and wider, sinusoidal topography instead of more localized hyperbolic profiles (6) here, along with a different set of control parameters, including a larger value for the Rossby radius of deformation. These differences may also be behind apparent lack of multiple "zonal" and "blocked" steady states in the present version of the model (cf. Charney and DeVore 1979). Therefore, our hypothesis about possible nonlinear sensitivity of the downstream impacts of the jet interacting with a TC-like singular vortex (SV) — in which this interaction would result in a transition between two such states — did not pan out. Therefore, in all cases of SV–jet interaction, discussed next, the jet perturbations due to vortex die out upon the SV's leaving the jet region, or are permanently

perturbed in the situations where the vortex is captured in the quiescent region on the lee side of the mountain towards the end of numerical experiment (see further details below). The maximum perturbations are achieved during the period the vortex is situated within the jet and can thus be expected to be most pronounced in the cases where this period is the longest.

3b. Interaction of a Singular Vortex with the Jet

We next performed numerical experiments in which, on top of each wavy steady state discussed in section 3a, a cyclonic SV was introduced south of the jet, at the distance of $5R_d$ from the axis of the channel. We used six different starting SV positions in longitude, situated at distances $-10R_d, -5R_d, -2.5R_d, 0, 2.5R_d, 5R_d$ from the center of the channel. Five of those positions ($-5R_d, -2.5R_d, 0, 2.5R_d, 5R_d$) sample the region of the climatological wave's secondary trough located in between the two mountains, where the interaction of SV with topography are minimized (see Fig. 5). The sixth initial position ($-10R_d$) is chosen to be on the lee side of the left mountain, in the region of the climatological wave's main trough. For this location, both the SV–mean-flow interactions and SV interactions with topography are likely to be important at all times. It is also worth noting that the same fixed set of initial conditions was used for all climatological states in Fig. 5 despite the latitudinal placement of the stationary wave exhibited slight differences depending on the width of the jet. Finally, recall that we used the SVs of three different intensities: weak, intermediate-strength, and intense SV (see Table 1). We start the discussion with the analysis of the SV trajectories in subsection i) and then proceed to analyze the vortex-induced perturbations to the regular flow in subsection ii).

i) Vortex trajectories

The self-propelled motion of the SV in the environment with the gradient of ambient potential vorticity occurs via generation of Rossby waves, whose near-field expression creates the dipolar beta-gyres that advect the vortex (Reznik 1992). On the beta-plane without the mean flow, the motion of the cyclone is initially northward and then northwestward (Kravtsov and Reznik 2019). The presence of the strictly zonal mean flow modifies the effective beta-parameter (Reznik and Kravtsov 2021; Kravtsov and Reznik 2023) and leads to the phenomenon of eddy entrapment on the prograde side of zonal jets if the effective beta parameter vanishes at some latitude (Reznik and Kravtsov 2024). While similar physics are at work in the present case, the addition of zonal-flow nonuniformities and, perhaps more substantially, topography effects is bound to modify this expected behavior by introducing the associated spatial variations in the background potential vorticity.

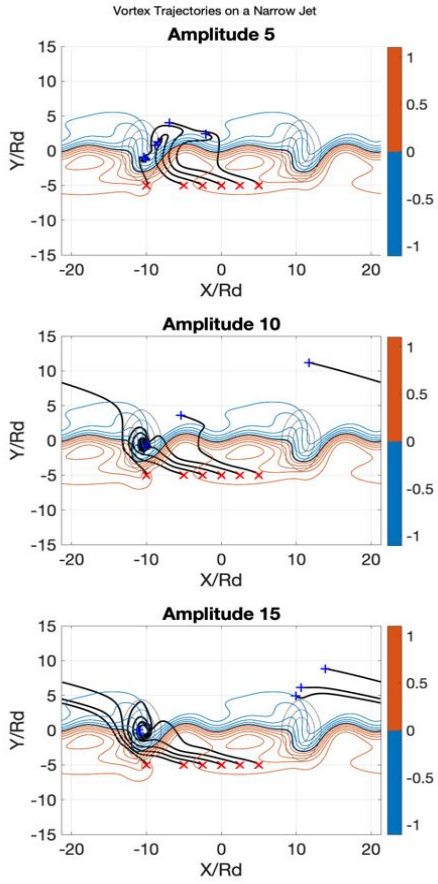

Figure 6: Trajectories of SVs of different intensities (black curves) for the narrow-jet climatological state of Fig. 5 (top plot), also replotted here as contours for convenience. Red x-symbols indicate the initial locations of the SV, while blue + symbols — the final location of each vortex. Top: weak SV; middle: intermediate-strength SV; bottom: strong SV.

For example, the initial evolution of a weak SV vortex placed to the south of the narrow jet in the central region of the channel (**Fig. 6**, top panel) follows the expected behavior, with the vortex starting northwestward motion in the region of the weak zonal flow prior to turning north while crossing the jet and, finally, exhibiting, again, a stronger deflection to the west when leaving the jet's core. Of the six trajectories considered here, only the two rightmost trajectories remain far away from the mountain regions throughout the course of the experiment, while others end up in a near-stationary position over the lee side of the upstream mountain. While this stationary behavior is interesting, we here focus on the dynamics of the vortex interaction with midlatitude trough in the climatological stationary wave, rather than in the interaction of the

vortex with topography, so we'll leave the analysis of the stagnating cyclones over topography to future work.

The comparison of the two trajectories in the valley between the two mountains highlights a difference between the vortex behavior depending on where exactly it enters the jet. The rightmost initial position of the vortex is associated with the trajectory that enters the jet exactly at the location of the secondary trough in the climatological stationary wave (namely, the trough in-between the mountains), crosses the jet quickly while moving directly northward and finally turns northwestward in the quiescent region north of the jet. In contrast to this behavior, the SV position initialization a bit further to the west from the first initial position results in a trajectory that enters the jet in the region of the ridge just upstream of the mid-channel trough. In this case, the vortex is able to resist the jet's advection less efficiently (due to the corresponding variations in the effective beta-parameter for sure) and is washed downstream before leaving the jet, thus spending more time in the jet's core region. It appears to be possible then that in this second case the downstream effects of the vortex on the climatological stationary wave will be stronger, as the vortex spend more time in the jet (which turned out not to be true; see subsection ii below!).

The higher-amplitude SVs over the narrow jet (Figs. 6, middle and bottom plots) are characterized by greater translational speeds against the mean flow across the domain. Depending on their initial position, they either end up captured on the lee side of the upstream mountain, or, alternatively, are able to dive around it and cross the jet to continue their westward path on the north side of the jet. Note again, that the only case in which the SV was able to spend substantial time within the jet's core before crossing the jet was the one with the intermediate-

strength SV at the easternmost initial placement (Fig. 6, middle panel). This SV, similar to the weak-vortex cases that spent substantial within the jet core (Fig. 6, top panel), entered the jet in the region of the upstream ridge in between the main and secondary troughs between the two mountains.

Similar general aspects of SV's behavior can be seen in the trajectories of an intermediate-strength vortex interacting with the wide jet (**Fig. 7**). The rightmost and leftmost initializations led to the final states associated with the SV cyclone's stagnation just downstream of the mountain on the prograde (cyclonic) side of the jet. Again, we'll leave the discussion of these states for the future. The remaining four trajectories initialized in the mid-channel region where all able to cross the jet while staying in the plateau region of the model basin but spent different amounts of time within the jet core. In particular, the trajectory that entered the jet in the location closest to the flat-region climatological-wave ridge (located at about $x = -2.5R_d$ to the west of the center of the channel) was washed downstream by the jet and spent the longest time within the jet core compared to the trajectories to both west and east of it. These latter

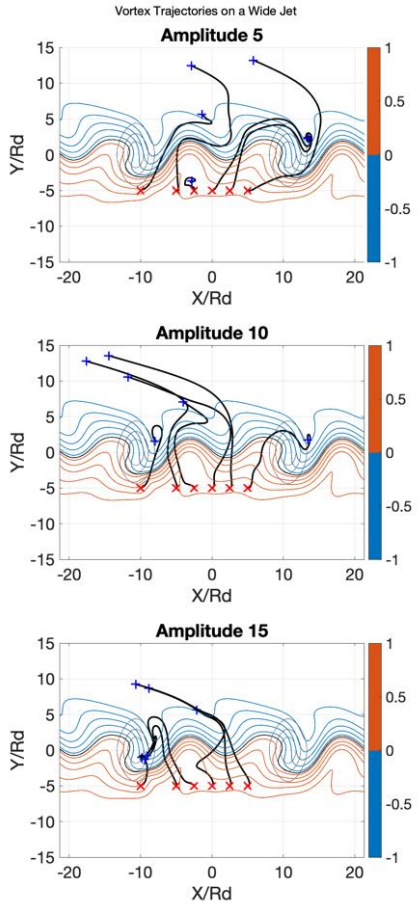

Figure 7: The same as in Fig. 6, but for the SVs interacting with the wide jet (Fig. 5, bottom plot).

trajectories entered the jet in the regions closer to the troughs or climatological jet, and resisted the jet's advection much more efficiently, while crossing the jet faster. Again, we hypothesize that the longer the SV is able to stay within the core of the jet, the stronger would be its potential downstream effects (but see subsection ii) below!).

Similar sets of cases can be found for weak and strong vortices (Fig. 7). These sets of cases are: [1] the vortex enters the jet in the region of the secondary trough, crosses the jet quickly, and moves more or less directly across the jet while doings so; [2] the vortex enters the jet close to the ridge just upstream of the secondary trough, is being washed downstream on the northern (anticyclonic) flank of the jet before leaving the jet region, leading to its longest

residence times within the jet core compared to other cases; [3] the vortex ends up in a stationary position on the lee side of either mountain. Note that the wide jet is much more efficient than narrow jet in counteracting the self-propelled northwestward vortex drift (strongest for large-magnitude vortices). Finally, one of the weak-vortex cases on wide jet is apparently characterized by the vortex trapped on the southern (cyclonic) flank of the wavy jet — this special case requires further inspection in the future.

Below, we pay particular attention to the sets of behavior [1] and [2] identified above. For the narrow jet, set [1] includes the cases of weak and intermediate-strength vortices initially at $x = 5R_d$, while set [2] consists of just one case — the weak vortex initially at $x = 2.5R_d$. For the wide jet, set [1] is represented by cases of the intermediate-strength vortex initially at $x = 0$ and $2.5R_d$, as well as the intense vortex at $x = 0, 2.5R_d$ and $5R_d$. Set [2] includes cases: weak vortex with $x = -5R_d$, as well as the intermediate-strength vortex with $x = -2.5R_d$ and $-5R_d$.

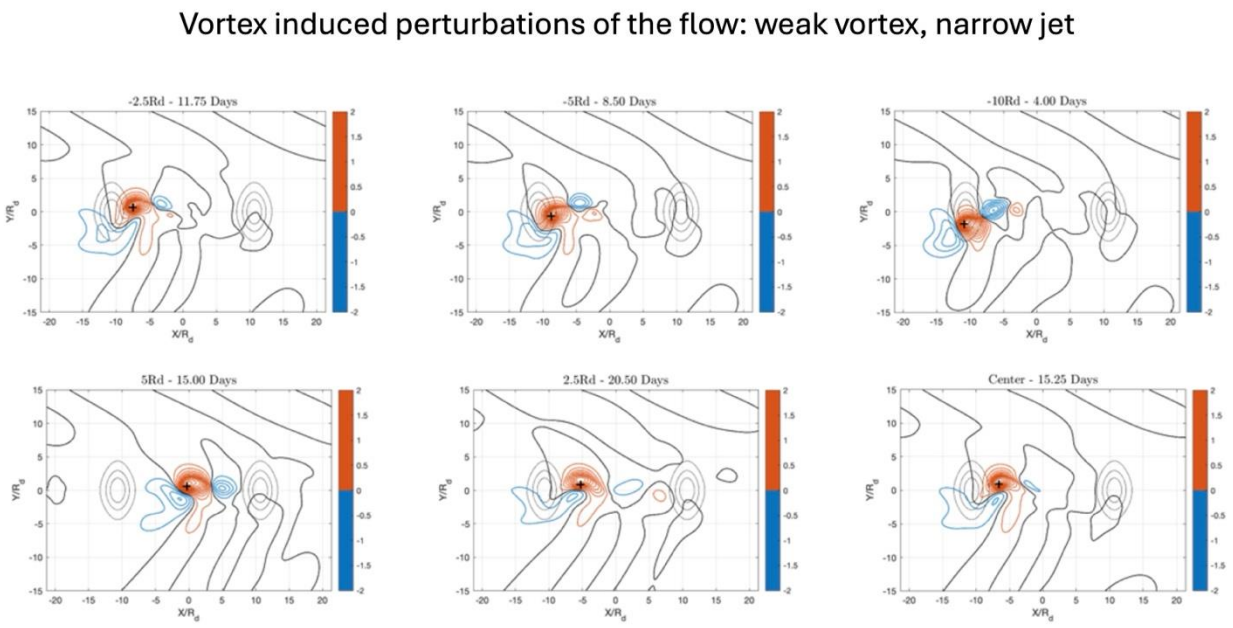

Figure 8: Maximum vortex-induced streamfunction perturbations for the case of weak vortex and narrow jet. The x-symbols show the position of the vortex. The time (from the start of the experiment) at which the maximum perturbation occurred in each case is shown in the panel captions, along with the initial position of the vortex. Streamfuction units are $U_0 R_d/m$, red and blue contours denote negative and positive perturbations, zero contour is black, contour interval is 0.1. Mountains are shown as thin black contours with the contour interval of 0.2.

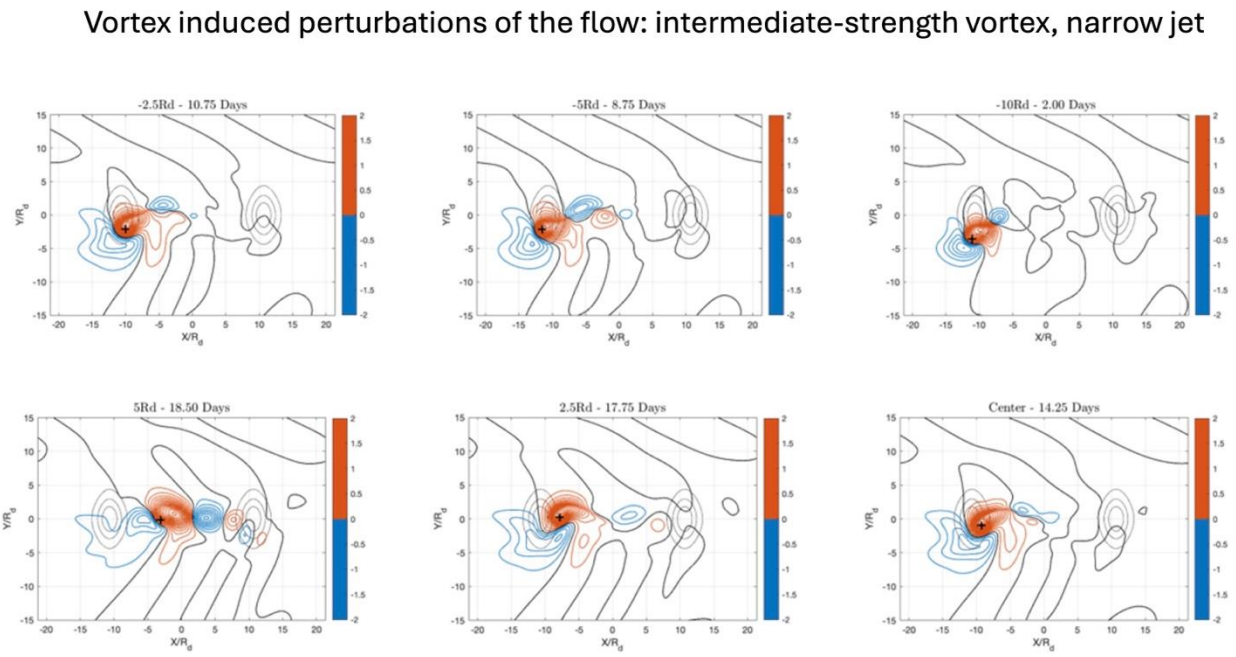

Figure 9: The same as in Fig. 8, but for the intermediate-strength vortex.

ii) Vortex-induced downstream perturbations of the jet

To measure the effect of the vortex on the downstream structure of the mean flow, we computed the vortex-induced regular streamfunction field by subtracting the initial value of the regular streamfunction in the beginning of the experiment (which characterizes stationary wave's steady state in the simulations without the vortex) from the full regular streamfunction in the course of each simulation with the vortex. The particular characteristic we focus on is the maximum vortex-induced perturbation. We also noted, for each case, the time elapsed from the beginning of each experiment to the occurrence of this maximum perturbation. To match the previous discussion, we begin our analysis with the narrow-jet simulations (see **Fig. 8** for the

weak-vortex case and **Fig. 9** for the intermediate-strength vortex). Generally, the timing and meridional location of the maximum vortex-induced perturbation in all cases approximately corresponds to the moment the vortex crosses the jet axis. The perturbation is always characterized by the main regular anticyclone that embeds the SV, which reflects the tendency of the full (regular+singular) vortex to weaken due to the dispersion by Rossby waves the vortex radiates (Kravtsov and Reznik 2019). In most cases the Rossby wave train generated by the vortex consists predominantly of this central anticyclonic lobe and two secondary cyclones on either side of it, with the orientation of this tripole being dependent on the positioning of the vortex with respect to the jet's stationary wave and the basin's topographic features.

Omitting the cases of vortex interaction with topography, we are left, for the narrow jet in Fig. 8, with two cases of trajectories over the flat region of the model basin. One of these cases, with vortex started at $x = 5R_d$ belongs to category [1] (direct, relatively fast crossing of the jet) and the one started at $x = 2.5R_d$ — to category [2] (slower meridional translation across the jet, with substantial downstream advection upon crossing the jet axis). Somewhat counterintuitively, case [1], while indeed reaching the maximum perturbation earlier than case [2], as expected from the analysis of the trajectories in Fig. 6 (top), generates a *stronger*, in magnitude, jet perturbation compared to that of case [2]. In the case [1], this perturbation is *out of phase* with the stationary wave and thus tends to make the flow more zonal as the vortex crosses the jet. The magnitude of the vortex-induced perturbation for this case quickly grows with the intensity of the vortex, as exemplified by a fairly intense wave in Fig. 9 (for case [1] initialization $x = 5R_d$). By contrast, case [2] is associated with the vortex producing perturbations in phase with the zonal nonuniformities of the climatological stationary wave, thus enhancing this stationary wave downstream. These findings may be related to the phenomenon of resonance, or "phase-locking"

of the vortex-induced perturbations with climatological quasi-stationary wave noticed earlier (see, for example, Keller et al. 2019).

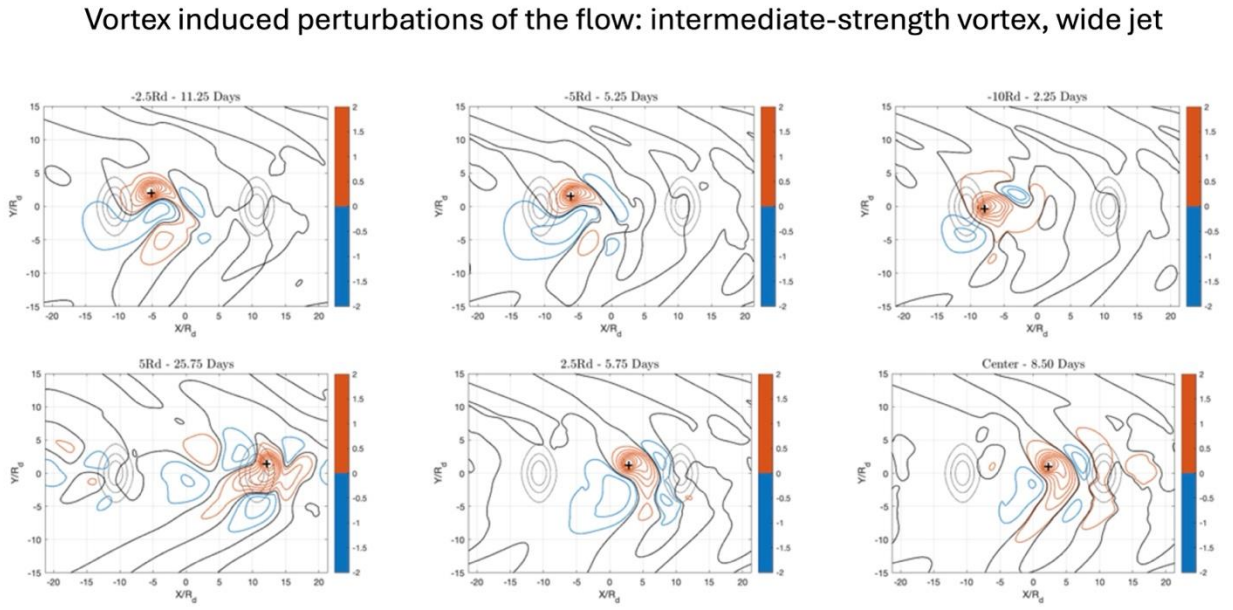

Figure 10: The same as in Fig. 8, but for the intermediate-strength vortex on a wide jet.

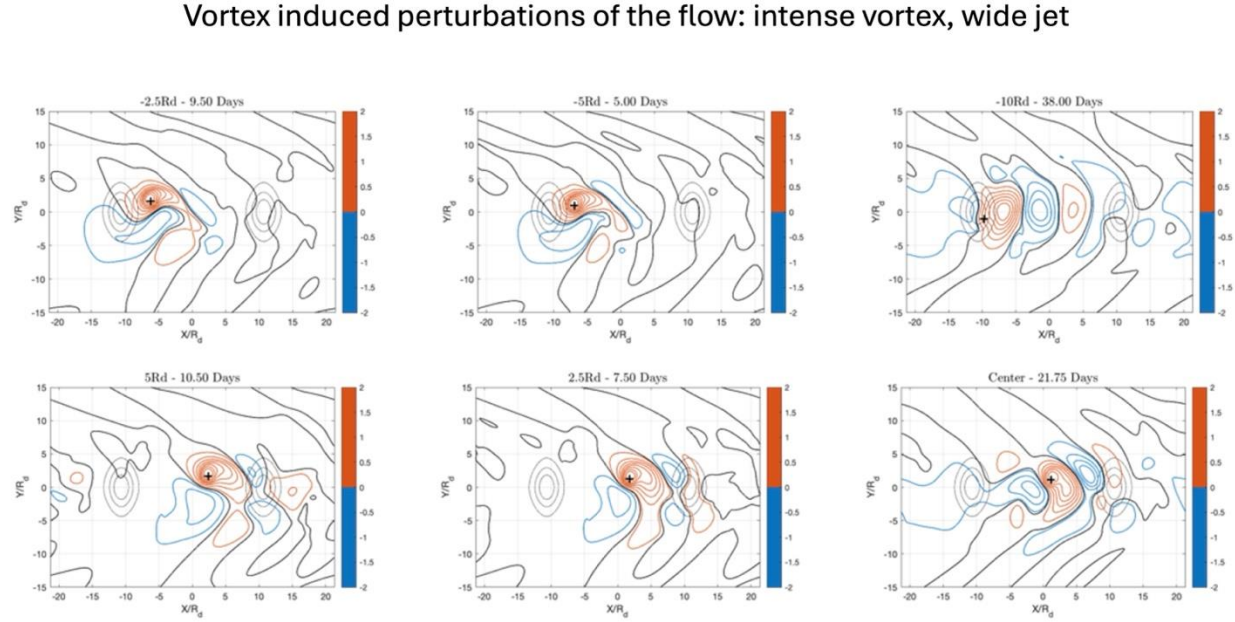

Figure 11: The same as in Fig. 8, but for the intense vortex on a wide jet.

Recall that for the wide jet, set [1] is represented by cases of the intermediate-strength vortex initially at $x = 0$ and $2.5R_d$, as well as the intense vortex at $x = 0, 2.5R_d$ and $5R_d$. Set [2] includes cases: weak vortex with $x = -5R_d$, as well as the intermediate-strength vortex with $x = -2.5R_d$ and $-5R_d$. The anomalies associated with these cases shown in **Figs. 10** (for intermediate-strength vortex) and **11** (for intense vortex). It seems that in the case of the wide jet the sensitivity of the vortex-induced maximum perturbations to the vortex intensity is not as large as that for the narrow-jet case: all of the set [1] cases mentioned above produce the anomalies of similar spatial structure and magnitude. The vortex trajectory associated with the largest and the most spread-out anomalies corresponds to the case of intense vortex with $x = 5R_d$ (Fig. 11, bottom right), in which the vortex-induced wave turns out to be almost exactly out of phase with the stationary wave and reaches maximum magnitude later than in other cases,

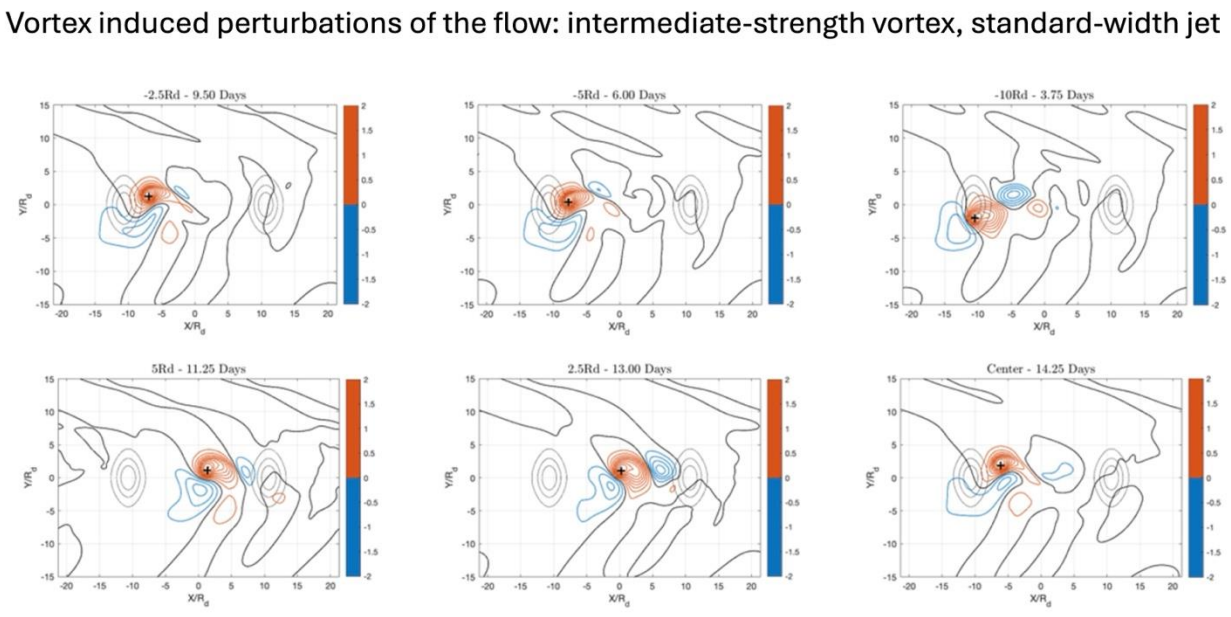

Figure 12: The same as in Fig. 8, but for the intermediate-strength vortex on a standard-width jet.

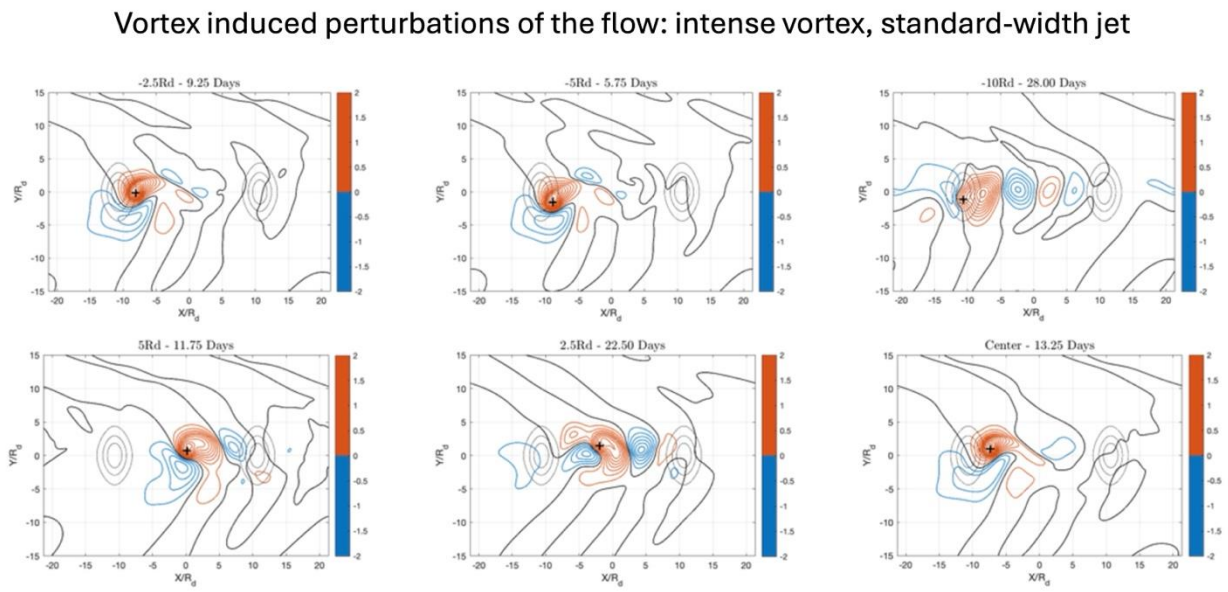

Figure 13: The same as in Fig. 8, but for the intense vortex on a standard-width jet.

indicating the longest duration of the SV–jet interaction; compare this, again, with Keller et al.'s (2019) concept of phase-locking and resonance. The set [2] cases for the intermediate-strength vortex (Fig. 10) also offer a complementary view of the difference between the two sets of possible regimes [1] and [2] of eddy–stationary wave interaction. Namely, the associated tripole of anomalies consists of a meridionally oriented dipole, with a secondary cyclone south of the main anticyclone that contains the SV, and a much weaker cyclone to the east of it, thus producing a fairly weak downstream enhancement of the climatological stationary wave. By contrast, the set [1] cases of the vortex anomalies entering the jet in the region of climatological trough, produces more zonally-extended anomalies out-of-phase with the climatological wave, which thus tend to substantially weaken the latter wave.

The characteristic signatures of the two interaction scenarios described above make it easy to ascribe the various cases for the interaction of the SV with the standard-width jet (**Figs. 12 and 13**). In particular, the intermediate-strength vortex near-resonant case [1] is clearly the one with $x = 2.5R_d$, based on the largely zonally oriented, persistent (long-lived) wave pattern out of phase with climatological wave, while the persistent case initialized in the center of the channel is representative of the interaction scenario [2], with an in-phase reinforcement of the climatological wave confined to the region of the SV's immediate vicinity (Fig. 12). The most spectacular set [1] resonant case is found for the intense vortex placed initially at $x = 2.5R_d$ (Fig. 13).

4. Summary, Discussion, and Outlook

In this study we considered, in an idealized model, interactions of a cyclone with a wavy mid-latitude jet. The model used a classical 1.5-layer quasi-geostrophic formulation with mean flow and bottom topography and was forced by the relaxation to the radiative equilibrium profile (see section 2). The cyclone's representation was done in the framework of a singular vortex whose shape was fixed in the course of the system's evolution (Reznik 1992). When inserted in the pre-existing steady background flow with a gradient of potential vorticity (including the cases without the mean jet and/or topography), the cyclone generates an additional, induced field and radiates Rossby waves, which interact with the cyclone and result in the cyclone's self-propagation. This interaction is modified in the presence of topography and involves, among other things, the background jet's perturbations downstream of the initial interaction. The goal of this work was to document possible regimes of such interaction and study their sensitivity to the model parameters and, in particular, to the initial positioning of the cyclone with respect to the preexisting wavy mid-latitude jet.

We first generated a set of wavy steady states in the model without the vortex, using the mean jets of different widths and intensities. These steady states produce a climatological stationary wave characterized by the two main troughs just downstream of each mountain and a secondary ridge/trough couplet in between the mountains. The magnitude of non-zonal undulations in the climatological wave was found to grow with the jet's width.

We next launched, in the background of climatological stationary waves described above, the SVs of different intensity using a set of initial positions that sampled the locations south of the jet in the valley between the two mountains. We found three distinct regimes of the vortex behavior: [1] the vortex enters the jet in the region of the secondary trough, crosses the jet quickly, and moves more or less directly across the jet while doings so; [2] the vortex enters the jet close to the ridge just upstream of the secondary trough, is being washed downstream on the northern (anticyclonic) flank of the jet before leaving the jet region, often leading to its longest residence times within the jet core compared to other cases; [3] the vortex ends up in a stationary position on the lee side of either mountain.

Our research focus here is on the interaction of the cyclones with the climatological stationary wave away from the mountain regions. Therefore, we concentrated on the analysis of cases belonging to the categories [1] and [2] above, and left the analysis of regime [3] for the future. We found that the regime [1], with the vortex entering the jet in the location of the climatological trough, is characterized by the most pronounced effect of the vortex on the preexisting flow. Here the vortex generates a zonally oriented wavelike regular perturbation flow field which is out of phase with the climatological wave and thus tends to make the jet's flow more zonal. The vortex itself resists the downwind advection by the background flow and is thus able to move directly northward across the climatological jet; the resulting translational motion

can be quite slow, indicating that the regime [1] is a self-sustained configuration with the vortex persistently staying in the region of the climatological wave's trough to keep generating the out-of-phase anomalies that can extend far upstream and downstream of this trough.

On the other hand, regime [2], while often characterized by the longest residence times of the vortex within the jet's core, only produces much weaker and more localized perturbation-flow anomalies compared to those of regime [1]. These anomalies occur, mainly, in the vicinity of the secondary climatological ridge in-between the mountains, where they form a meridionally oriented dipole, whose northern anticyclonic lobe tends to cancel the background flow's climatological ridge. An even weaker cyclonic anomaly further downstream is also in phase with the secondary climatological trough there. In this regime, the long residence times of the cyclone entering the jet in the location of the climatological ridge are apparently due to smaller effective beta-parameter (gradient of ambient potential vorticity) and, hence, weaker regular-flow anomalies generated by the cyclone, weaker meridional translational speeds, and weaker ability of the cyclone to counteract the advection by the background eastward jet, as evidenced by its eventual eastward migration on the northern flank of the jet.

Our results are consistent with previous studies of vortices acting as a long-lived "local wave makers," especially in the cases of vortices that became trapped within a trough, prolonging their time within the flow to affect downstream perturbation wave patterns (Riemer et al. 2008, Keller et al. 2019). These perturbations provide context of the level of interaction between approaching cyclones to the midlatitude flow generated pronounced ridge–trough couplets and additional cyclones further downstream (Jones et al. 2003, Riemer et al. 2008). Our findings of the regime [1]'s optimality in terms of being able to generate maximum perturbations of the pre-existing jet are reminiscent of the earlier concept of "phase-locking," coined by

numerous studies, referring to the situation when the approaching cyclone moves in tandem with the upstream trough in a self-sustained way that maximizes the coupling between the mean-flow wavy jet and the incoming cyclone (Jones et al. 2003, Riboldi et al. 2019, Keller et al. 2019).

Future extensions of this study may include generalizations to baroclinic quasi-geostrophy in, say, two-layer representations, which would certainly add a much larger degree of realism by accounting for important dynamics of baroclinic instability entirely missing from the present formulation, as well as for a more realistic vertical structure of the cyclone impinging onto the wavy mid-latitude jet. Including the moist dynamic in such a multi-layer quasi-geostrophic formulation is also possible (Kravtsov et al. 2022). Such idealized studies will continue to complement the analyses and insights obtained via more realistic models to help obtain a holistic view of various aspects of the Earth's system dynamics.

REFERENCES

Archambault, H. M., L. F. Bosart, D. Keyser, and J. M. Cordeira, 2013: A Climatological analysis of the extratropical flow response to recurving western North Pacific tropical cyclones. *Mon. Wea. Rev*., **141**, 2325–2346, https://doi.org/10.1175/MWR-D-12-00257.1.

Archambault, H. M., D. Keyser, L. F. Bosart, C. A. Davis, and J. M. Cordeira, 2015: A composite perspective of the extratropical flow response to recurving western North Pacific tropical cyclones. *Mon. Wea. Rev.*, **143**, 1122–1141, https://doi.org/10.1175/MWR-D-14-00270.1.

Aiyyer, A., 2015: Recurving western North Pacific tropical cyclones and midlatitude predictability. *Geophysical Research Letters*, **42**, 18, 7799-7807, https://doi.org/10.1002/2015GL065082.

Charney, J. G. and DeVore, J. G., 1979: Multiple flow equilibria in the atmosphere and blocking. *Journal of the Atmospheric Sciences*, **36,** 7, 1205-1216, https://doi.org/10.1175/1520-0469(1979)036<1205:MFEITA>2.0.CO;2.

Evans, C., and Coauthors, 2017: The extratropical transition of tropical cyclones. Part I: Cyclone evolution and direct impacts. *Mon. Wea. Rev.*, **145**, 4317–4344, https://doi.org/10.1175/MWR-D-17-0027.1.

Finocchio, P. M., and J. D. Doyle, 2019: How the speed and latitude of the jet stream affect the downstream response to recurving tropical cyclones. *Mon. Wea. Rev.*, **147**, 3261–3281, https://doi.org/10.1175/MWR-D-19-0049.1.

Ferreira, R. N., and W. H. Schubert, 1999: The Role of tropical cyclones in the formation of tropical upper-tropospheric troughs. *J. Atmos. Sci.*, ***56***, 2891-2907. https://doi.org/10.1175/1520-0469(1999)056<2891:TROTCI>2.0.CO;2

Grams, C. M., and S. R. Blumer, 2015: European high-impact weather caused by the downstream response to the extratropical transition of North Atlantic Hurricane Katia (2011). *Geophys. Res. Lett.*, **42**, 8738–8748, https://doi.org/10.1002/2015GL066253.

Jones, S. C., and Coauthors, 2003: The extratropical transition of tropical cyclones: Forecast challenges, current understanding, and future directions. *Wea. Forecasting*, **18**, 1052 1092, https://doi.org/10.1175/1520-0434(2003)018,1052:TETOTC.2.0.CO;2.

Keller, J. H., and Coauthors, 2019: The extratropical transition of tropical cyclones. Part II: Interaction with the midlatitude flow, downstream impacts, and implications for predictability. *Mon. Wea. Rev.*, **147**, 1077–1106, https://doi.org/10.1175/MWR-D-17 0329.1.

Kravtsov, S., and S. Gulev, 2013: Kinematics of eddy–mean-flow interaction in an idealized atmospheric model. *J. Atmos. Sci.*, **70**, 2574–2595. https://doi.org/10.1175/JAS-D-12-0309.1

Kravtsov, S., I. Rudeva, and S. Gulev, 2015: Reconstructing sea-level pressure variability via a feature tracking approach. *J. Atmos. Sci.*, **72**, 487–506, https://doi.org/10.1175/JAS-D-14-0169.1.

Kravtsov, S., and Reznik G. M., 2019: Numerical solutions of the singular vortex problem, *Phys. Fluids*, **31**, 066602-1 – 066602-17. https://doi.org/10.1063/1.5099896.

Kravtsov, S., and Reznik G. M., 2020: Monopoles in a uniform zonal flow on a quasi-geostrophic beta-plane: Effects of Galilean non-invariance of the rotating shallow water equations. *J. Fluid Mech.*, **909**, A23. https://doi.org/10.1017/jfm.2020.906.

Kravtsov, S., and G. M. Reznik, 2023: Quasi-geostrophic monopoles in a sheared zonal flow: Influence of the beta-effect and variable shear, *Physics of Fluids*, **35**, 016606, https://doi.org/10.1063/5.0131328.

Kravtsov, S., I. Mastilovic, W. K. Dewar, A. McC. Hogg and J. R. Blundell, 2022: A Moist Quasi-Geostrophic Coupled Model: MQ-GCM2.0. *Geosci. Model Dev.*, **15**, 7449–7469, https://doi.org/10.5194/gmd-15-7449-2022

Legras, B., and M. Ghil, 1985: Persistent Anomalies, Blocking and Variations in Atmospheric Predictability. *J. Atmos. Sci.*, **42**, 433–471, https://doi.org/10.1175/1520-0469(1985)042<0433:PABAVI>2.0.CO;2.

Löptien, U., and E. Ruprecht, 2005: Effect of synoptic systems on the variability of the North Atlantic Oscillation. *Mon. Wea. Rev.*, **133**, 2894–2904. https://doi.org/10.1175/MWR3007.1

Riboldi, J., C. M. Grams, M. Riemer, and H. M. Archambault, 2019*:* A phase locking perspective on Rossby wave amplification and atmospheric blocking downstream of recurving western North Pacific tropical cyclones. *Mon. Wea. Rev.*, ***147***, 567–589, https://doi.org/10.1175/MWR-D-18-0271.1.

Riemer, M., S. C. Jones, and C. A. Davis, 2008: The impact of extratropical transition on the downstream flow: An idealized modelling study with a straight jet *Quart. J. Roy. Meteor. Soc.* **134**, 69–91. https://doi.org/10.1002/qj.189

Reznik, G. M., 1992: Dynamics of singular vortices on a β-plane. *J. Fluid Mech.*, **240**, 405–432. https://doi.org/10.1017/S0022112092000144.

Reznik, G. M. and Kizner, Z., 2010: Singular vortices in regular flows. *Theor. Comput. Fluid Dyn.*, **24**, 65-75. DOI 10.1007/s00162-009-0150-5.

Reznik, G., and S. Kravtsov, 2021: Monopoles in a zonal flow with constant shear on a quasi-geostrophic *f*-plane: Effects of Galilean non-invariance. *Physics of Fluids*, **33**, 116606; https://doi.org/10.1063/5.0069722

Riemer, M., S. C. Jones, and C. A. Davis, 2008: The impact of extratropical transition on the downstream flow: An idealized modelling study with a straight jet. *Quart. J. Roy. Meteor. Soc*. **134**, 69–91. https://doi.org/10.1002/qj.189.

Schwierz, C., S. Dirren, and H. C. Davies, 2004: Forced waves on a zonally aligned jet stream. *J. Atmos. Sci.*, ***61***, 73–87. https://doi.org/10.1175/1520-0469(2004)061<0073:FWOAZA>2.0.CO;2

Swanson, K. 2008: Storm Track Dynamics. In: The Global Circulation of the Atmosphere, Chapter 4, https://api.semanticscholar.org/CorpusID:7992379

Wirth, V., M. Riemer, E. K. Chang, and O. Martius, 2018: Rossby wave packets on the midlatitude waveguide—a review. *Mon. Wea. Rev.*, **146**, 1965–2001. https://doi.org/10.1175/MWR-D-16-0483.1